PART II
Circumstellar Envelopes and Disks

THE STRUCTURE AND EVOLUTION OF ENVELOPES AND DISKS IN YOUNG STELLAR SYSTEMS

LEE G. MUNDY AND LESLIE W. LOONEY
University of Maryland at College Park

and

WILLIAM J. WELCH
University of California at Berkeley

This chapter presents an observational overview of the characteristics and evolution of young stellar systems that are forming singly or in loose clusters and groups. Starting with the nature of fragmentation and multiplicity in these environments, we look at the structure of envelopes and disks around the youngest stars and explore the evolution of these structures from the earliest stage of stellar core formation to the emergence of an optical star. Evidence for the kinematics of disks and large-scale flattened structures is discussed and placed in an overall context.

I. INTRODUCTION

The early evolution of young stellar systems is characterized by dramatic growth and change that take the system from a collapsing prestellar core to a revealed star with 90% or more of its final mass. During this period, the molecular core, which originally extended from several thousand to 10,000 AU, falls inward, feeding a central star and a circumstellar disk. In many cases the core forms two or more stars rather than a single star, and both circumstellar and circumbinary structures may form (see also the chapters by Bodenheimer et al. and Mathieu et al. in this volume).

This chapter focuses on observational studies of the environments of young, forming stars in isolated and loose group environments. By "isolated" we refer to both individual stars and multiple stellar systems that are forming at separations of 15,000 AU or more from other systems. This separation is large enough that neighboring systems do not compete gravitationally for material or interact tidally during formation, unlike the situation that occurs in cluster-mode star formation (Bonnell et al. 1997; see also the chapter by Clarke et al., this volume). This definition of "isolated" is broader than in many previous works, where the term refers only to studies of single-star formation (see, e.g., Shu et al. 1993). The reality is that multiplicity and grouping are common among young stars (Simon et al. 1992; Ghez et al. 1997; Patience et al. 1998). In fact, the median separation of main-sequence binaries (~30 AU; Duquennoy and Mayor 1991)

corresponds to less than an arcsecond in the nearest star-forming clouds; hence, it is often difficult to know whether a given system is single or multiple. A good example of this is the L1551 IRS5 system, which was initially considered a prototypical single-star system but now is argued to be a binary with a projected separation of 45 AU (Looney et al. 1997; Rodriguez et al. 1998).

The earliest stages of star formation, which take place before the formation of a stellar core, are covered in the chapter by André et al. in this volume. This chapter will concentrate on the environments of stellar systems which have formed a protostellar core. We will look at systems in stages of evolution from a deeply embedded protostar to a nearly uncovered young star.

II. FRAGMENTATION AND MULTIPLICITY

Molecular clouds are inhomogeneous on a wide range of scales. Facets of their structure can be observed utilizing molecular line and dust emission (cf. the chapter by Williams et al., this volume), but a complete understanding has proven elusive. The connection between structures within a cloud and the eventual formation of stars in that material is of particular interest here. Detailed studies indicate that the largest structures, containing hundreds to thousands of solar masses, are gravitationally bound as measured by the virial theorem, but most structures with ten solar masses or less are either not gravitationally bound or are bound only in the presence of a high external pressure (Bertoldi and McKee 1992; Williams and Blitz 1998). In the first case, the large structures must fragment into lower-mass cores to form stars; in the second case, it is unclear whether the cores are on the verge of gravitational collapse or whether they are transient unbound structures. Without knowledge of which pieces become stars, it is difficult to predict the distribution and multiplicity of the resulting stellar population.

An alternative approach for studying the star-forming capacity of clouds is to look at the distribution of the youngest embedded stars. These systems, which are still embedded in their natal cores, trace the number and distribution of bound cores that have formed stars over the last 10^5 to 10^6 years. The relative positions and extents of the cores provide information about the fragmentation process and the spatial scales of stellar clustering during formation (Motte et al. 1998; Testi and Sargent 1998). This information is different from that derived in cloud structure studies, where the star-forming capacity of the structures is uncertain, and from the results of studies of the distribution of young optical and near-infrared stars (Gomez et al. 1993; Simon 1997; Nakajima et al. 1998), where one sees the star formation history integrated over more than 10^6 years.

Recent wide-field continuum maps of a portion of the Perseus cloud NGC 1333 (Sandell and Knee 1998) and of the main ρ Ophiuchi cloud (Motte et al. 1998) provide good examples of the structure in active star formation regions. Figure 1 shows the $\lambda = 850\ \mu$m map of the NGC 1333

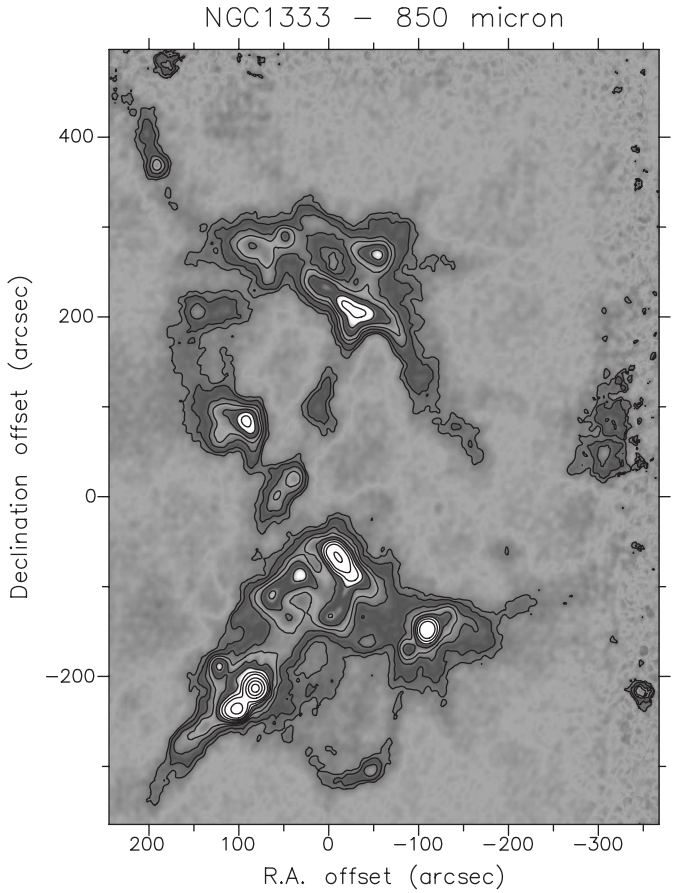

Figure 1. Map of the $\lambda = 850$ μm continuum emission from the NGC 1333 SVS13 region (G. Sandell and L. B. G. Knee, personal communication, 1998). The brightest emission appears as white in the grayscale image. The data were acquired with the Submillimetre Common User Bolometer Array (SCUBA) on the James Clerk Maxwell Telescope (JCMT).

region. The emission at $\lambda = 850$ μm arises primarily from dust. The amount of emission increases with increasing temperature and column density; hence, when young stars are present, bright peaks in the distribution closely trace the locations of young embedded stars. In Fig. 1, there are roughly 18 discrete peaks over an area of roughly 65 square arcminutes. The strongest peaks can be identified with known embedded systems: SVS 13, HH 1–2, NGC 1333 IRAS 2, NGC 1333 IRAS 4, and NGC 1333 IRAS 7. In ρ Ophiuchi, roughly 100 small-scale structures were identified.

Higher-resolution continuum images of many of these systems uncover substructure. For example, Chini et al. (1997) find three separate sources within the HH 1–2 system and the SVS 13 system (see also

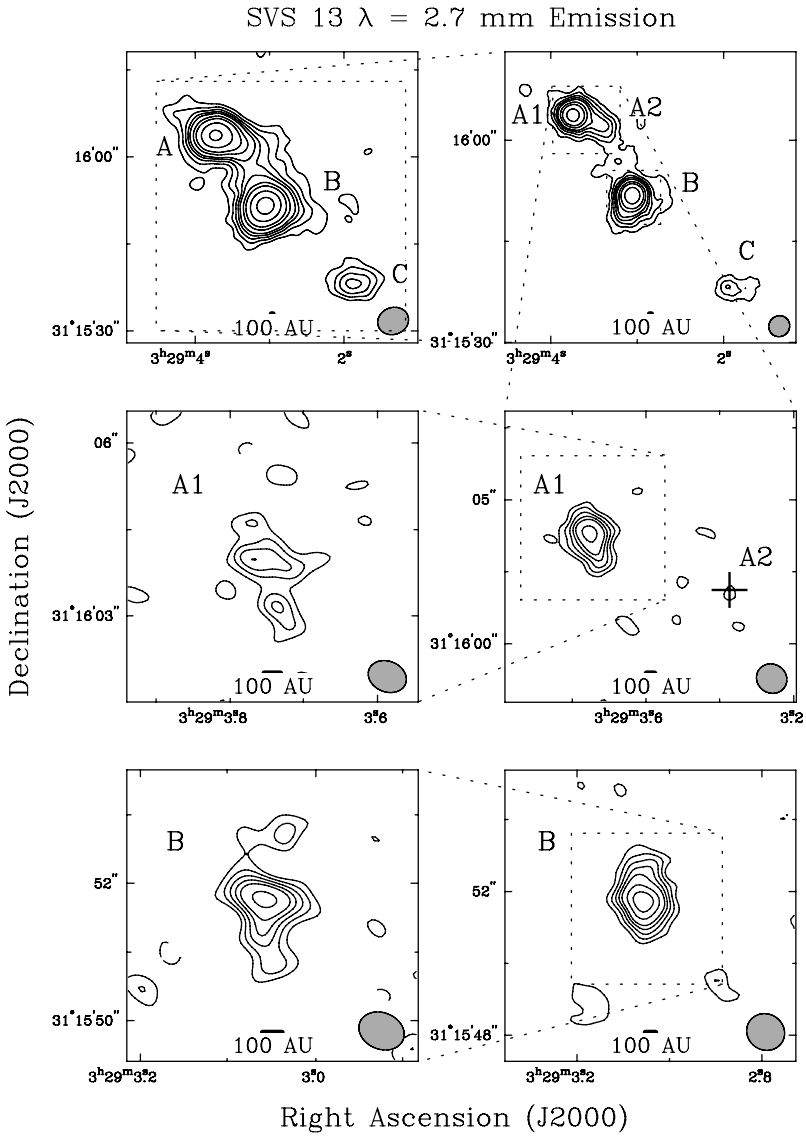

Figure 2. Images of the $\lambda = 2.7$ mm continuum emission from the NGC 1333 SVS13 region from Looney et al. (1998). The four upper panels show images of the system with increasing resolution: 5″ in the upper left, 3.1″ in the upper right, 1.1″ in the middle right, and 0.6″ in the middle left. The bars at the bottom of each panel show 100 AU linear distance. The lower two panels show 1.1″ (right) and 0.6″ (left) images of the SVS13B source. The source designations, A, B, and C, are indicated in the top two panels.

Bachiller et al. 1998); the NGC 1333 IRAS 4 system divides into four sources at arcsecond resolution (Sandell et al. 1991; Lay et al. 1995; Lefloch et al. 1998). Subarcsecond resolution images of several sources in this region confirm this multiplicity. Figures 2 and 3 show interferometric images of the SVS 13 and NGC 1333 IRAS 4 systems; the six panels

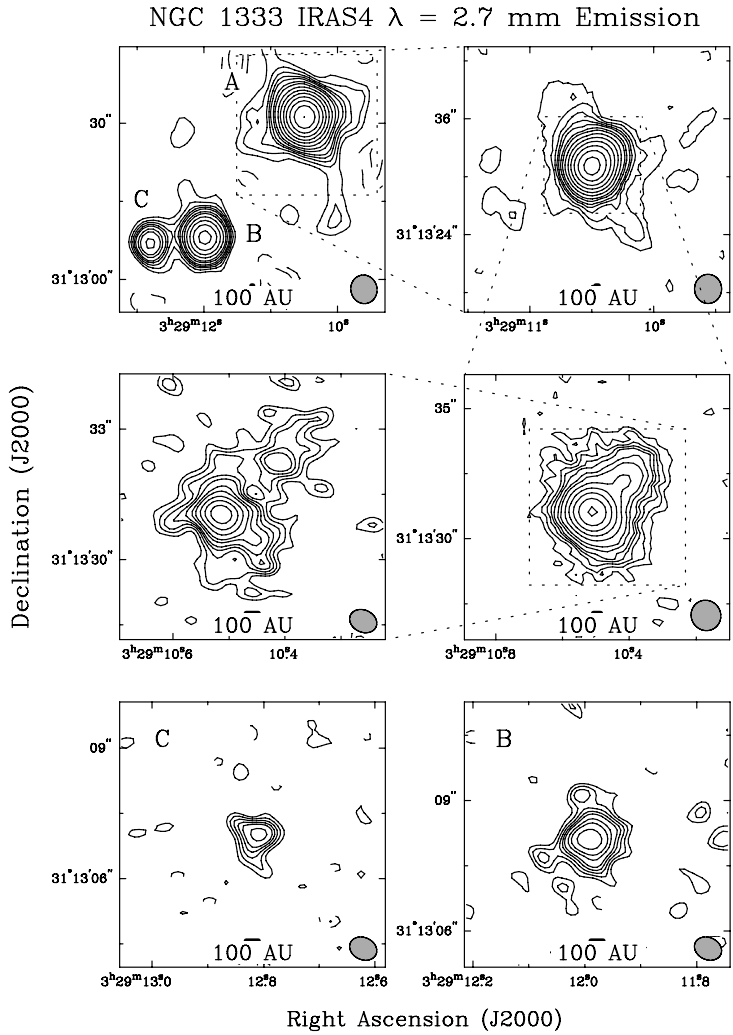

Figure 3. Images of the $\lambda = 2.7$ mm continuum emission from the NGC 1333 IRAS 4 region from Looney et al. (1998). The four upper panels show images of the system with increasing resolution: 5.2″ in the upper left, 3.0″ in the upper right, 1.1″ in the middle right, and 0.6″ in the middle left. The bars at the bottom of each panel show 100 AU linear distance. The upper panels are centered on IRAS 4A; the lower two panels show 0.6″-resolution images of IRAS 4B and 4C. The source designations, A, B, and C, are indicated in the top left panel.

within each figure range in resolution from roughly 5″ to 0.6″ (Looney et al. 1998). Multiplicity on a range of scales is clearly present. These images are part of a 0.6″-resolution millimeter-wavelength survey of six deeply embedded systems in Ophiuchus and Perseus (Looney et al. 1998) that found that all systems were multiples on a $\leq$10,000 AU scale, with a total of seventeen sources identified in the six systems. Several systems were binary on 100–700 AU scales. Due to the resolution limit of the survey, little is known about multiplicity on scales $<$100 AU.

Morphologically, three types of multiple systems can be identified in the abovementioned works: independent envelope, common envelope, and common disk systems. The characteristics of the systems are defined by the distribution of the circumstellar material. Independent envelope systems exhibit clearly distinct centers of gravitational concentration with separations of $\geq$6000 AU; the components are within a larger surrounding core of low-density material. Common envelope systems have one primary core of gravitational concentration, which breaks into multiple objects at separations of 150–3000 AU. Common disk systems have separations of $\leq$100 AU and typically have circumbinary disklike distributions of material. Table I summarizes these characteristics.

There are several clear connections between these morphological distinctions and other works. The study of the separation distribution of optical binaries by Larson (1995) found a knee in the distribution at 0.04 pc (8250 AU), which was posited to correlate with the Jeans size. Larson suggested that systems on that scale and larger were formed by fragmentation and separate collapse, exactly the structure found in the independent envelope systems. This scenario of prompt initial fragmentation is not new (see, e.g., Larson 1978; Pringle 1989; Bonnell et al. 1991); it was discussed recently by Bonnell et al. (1997) in the context of small cluster formation. The critical issue is that the collapse is initiated in a system that contains multiple Jeans masses in a weakly condensed configuration; one example of such a system would be a prolate Gaussian distribution with several Jeans masses along the long axis and one Jeans mass across the short axis. This mass concentration before fragmentation is needed to get sufficient mass on the appropriate size scale for systems with $\sim$6000 AU separations. At separations much larger than 6000 AU, independent inside-out or quasistatic collapse from the original cloud (Shu 1977; Fiedler and Mouschovias 1993; Galli and Shu 1993) is viable.

TABLE I
Characteristic Scale of Multiplicity

Property	Scale
Independent envelope	$\geq$6000 AU
Common envelope	150–3000 AU
Common disk	$\leq$100 AU

The common envelope systems can be linked with models for the fragmentation of moderately centrally condensed spherical systems (Burkert and Bodenheimer 1993; Boss 1995, 1997; the chapter by Bodenheimer et al., this volume). In this case, the models find fragmentation in the dense central region within an overall single core. The primary requirement for fragmentation is that the central region have a fairly flat distribution; evidence of this flat region is erased soon after the collapse occurs. Thus, the forming multiple system is embedded within a single centrally condensed core. Finally, the common disk systems are similar to models of high-angular-momentum systems (Artymowicz and Lubow 1994; Bate and Bonnell 1997). The close stellar systems represent the fragmentation of early disks. The distribution of material between circumstellar and circumbinary structures depends on the angular momentum of the infalling material.

III. THE STRUCTURE OF ENVELOPES

The primary parameters that define the characteristics of a circumstellar envelope are size, density structure, temperature structure, mass, and kinematics. These characteristics can, in principle, be observationally determined from the molecular emission associated with the gas and the thermal continuum emission from the dust. There are, however, significant difficulties and uncertainties associated with the various methods available for deriving these parameters.

A. Molecular Emission

Molecular emission arises from a variety of species present in the gas. Differences in molecular structure and abundance make selected species particularly useful in determining specific physical parameters. For example, ^{13}CO or $C^{18}O$ are generally good H_2 column density tracers because their abundance is reasonably constant, they are easily thermalized, and the transitions are generally optically thin. Common molecules with large dipole moments, such as CS, H_2CO, HCN, and HCO^+, are good probes of the gas density and can be useful probes of the column density in some situations. Symmetric or slightly asymmetric top molecules, such as NH_3, H_2CO, and CH_3CN, provide measures of the gas temperature. The molecular line shapes yield information about the kinematics of the gas; the kinematics of the envelope is the focus of the chapter by Myers et al., this volume. In principle, by mapping the emission from several transitions in representative species from each of these key groups, one can derive a complete picture of the envelope structure (e.g., Fuller et al. 1995; Ladd et al. 1998).

Two examples of what can be done utilizing multiple molecular probes are provided by detailed work on B335 (Zhou et al. 1993; Choi et al. 1995) and IRAS 16293−2422 (Zhou 1995; Narayanan et al. 1998). B335 is an isolated globule forming a low-mass star, which is argued to be

currently undergoing collapse. The authors fitted multiple transitions of CS and H_2CO to the inside-out collapse model for the envelope (Shu 1977; Shu et al. 1993); they found that the $r^{-1.5}$ density distribution within the infall radius, and r^{-2} density profile beyond that radius, produced good fits to their line profiles and maps for an infall radius of 0.03 pc. IRAS 16293−2422 is a deeply embedded young binary system with a separation of about 750 AU. Zhou (1995) fits the inside-out collapse model to this system, and Narayanan et al. (1998) fit the rotating collapse solution of Terebey et al. (1984) to transitions of CS and HCO^+. The latter find that the data are best fitted for an infall radius of 0.03 pc.

It is important to note that such model fitting shows that the data are consistent with the model, but it does not prove that the model is unique. In a survey of embedded low-mass young stars, Hogerheijde et al. (1997) found that the HCO^+ emission from the envelopes was well described with either the inside-out collapse or by a simple power law density distribution with a power law index of 1 to 3.

B. Continuum Emission

Observations of the continuum from millimeter through mid-infrared wavelengths provide information about the dust distribution and temperature. The millimeter and submillimeter wavelengths are particularly good for determining the column density, because the emission is linearly dependent on dust temperature. Because of the exponential temperature dependence in the Planck function, the dust temperature is best determined from continuum observations from 450 μm to the mid-infrared wavelengths. Unfortunately, measurements of the column density and temperature structure are not decoupled from each other, so maps at several wavelengths spaced across the millimeter to mid-infrared regime and flux measurements covering the broad spectral energy distribution are essential. Physical density must be inferred for an assumed envelope geometry.

The simplest approach for modeling the dust emission is to assume a power law envelope (e.g., Adams et al. 1987; Walker et al. 1990; Adams 1991; Yun and Clemens 1991). In a power law envelope, the density and temperature are assumed to follow a power law dependence on radius: $\rho \propto r^{-p}$, and $T \propto r^{-q}$, respectively; the dust opacity is assumed to follow a power law in frequency: $\kappa_\nu \propto \nu^\beta$. At long wavelengths, where the Rayleigh-Jeans limit applies, the dust emission is then proportional to $\nu^{2+\beta} r^{-(p+q)}$. Modifications to the density power law have also been used, such as assuming the density distribution from Terebey et al. (1984). Such simplifying assumptions are very useful in situations where limited data are available or little detail is known about the source structure.

When a large body of data is available on an object, a full radiative transfer treatment is more appropriate and yields more realistic models. In such treatments, grain temperatures for a distribution of grain sizes are

calculated assuming a central heating source (Rowan-Robinson 1980; Wolfire and Cassinelli 1986; Butner et al. 1994). In these models, the temperature profile in the inner regions of the envelope rises more steeply than $r^{-0.4}$ and is not well represented by a single power law. In the outer parts of the envelope, the temperature profile is reasonably approximated by a power law, $r^{-0.4}$, until external heating from the ambient radiation field dominates. For low-luminosity sources, external heating can be important over a significant portion of the core (Motte 1998). In addition to solving for dust temperatures, the radiative transfer models allow consideration of more specific source geometry. For example, Men'shchikov and Henning (1997) model the L1551 IRS5 system utilizing a Gaussian core and power law density envelope with outflow cavities. With this multicomponent model they can fit observations including far-infrared maps, the broad spectral energy distribution, interferometer visibility data, scattered-light images, and dust polarization measurements.

An approach that measures the spatial structure more directly is to fit the visibilities measured by interferometers (Keene and Masson 1990; Lay et al. 1994; Looney et al. 1998). Interferometers intrinsically measure the Fourier transform of the sky brightness. The Fourier transform of the emission from an optically thin power law envelope, $F(r) \propto r^{-(p+q)}$, is the visibility amplitude, $V(d) \propto d^{(p+q-3)}$, where d is the (u,v) distance corresponding to the projected interferometer baseline length (Welch et al. 1999). This expression is valid for $1.5 < p + q < 3$, which is a reasonable range for expected parameters (Foster and Chevalier 1993; Wilner et al. 1995). Thus, the visibility is a power law in (u,v) distance. Different (u,v) distances trace different spatial scales in an object. Figure 4 shows

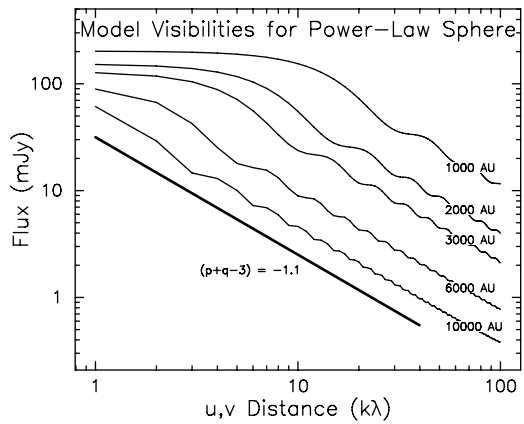

Figure 4. Plots of model visibilities for power law envelopes with different outer cutoff radii. The curves are labeled with the outer radius in AU. The lower thick line is the analytic request for an infinite power law distribution, as explained in the text. The envelope is optically thin.

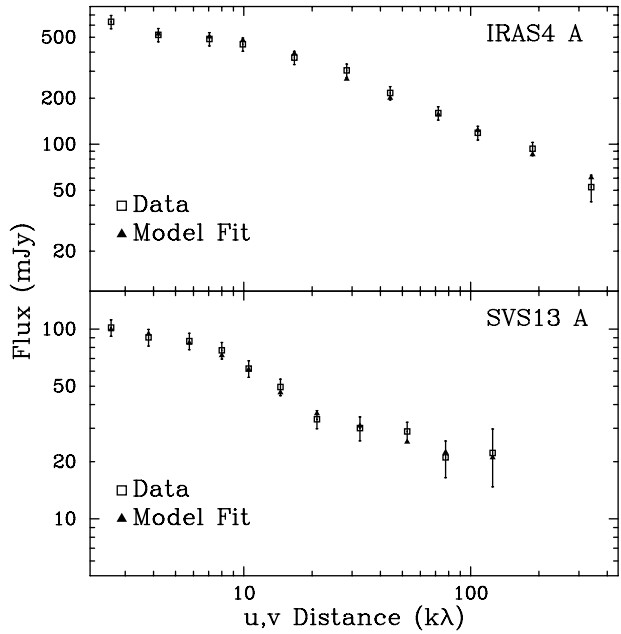

Figure 5. Plots of annular averaged (u, v) data and fits for the NGC 1333 IRAS 4A and NGC 1333 SVS 13A systems from Looney et al. (1998). The model parameters for the fit to IRAS 4A are density power law index = 1.8, outer radius = 2000 AU, point source flux = 22mJy, and envelope mass = 4.2 $M_\odot$. The model parameters for the fit to SVS 13A are density power law index = 1.6, outer radius = 4000 AU, point source flux = 18 mJy, and envelope mass = 0.8 $M_\odot$.

an example of model visibility amplitudes for an envelope with different outer radius cutoffs. The outer radius cutoffs cause the curves to flatten at smaller (u,v) distances, corresponding to bigger spatial scales, and the abrupt outer edge creates the oscillations with (u,v) distance. Because of these effects, more detailed modeling is valuable in deriving $p + q$.

Figure 5 shows the data and fits for two young embedded systems (Looney et al. 1998). In these fits to the real data, a central compact source is included, to represent a circumstellar disk embedded within the envelope, and the dust temperature is solved self-consistently. The best-fit density power law indexes for these two systems are in the range 1.2–2.0. The masses in the envelopes are 4.2 and 0.8 $M_\odot$ for IRAS 4A and SVS13A, respectively. If the fitted point sources are assumed to be HL Tauri type disks at the distance of Perseus, they correspond to masses of 0.08 to 0.15 $M_\odot$.

C. Difficulties and Broad Results

Methods for determining the structure of envelopes with embedded young stars are not as simple as they first appear. Often significant cross-

correlations between parameters in the models limit the ability to derive quantities. For example, density and temperature have a significant cross-correlation in molecular excitation calculations, and radial density law and outer radius cutoff are intertwined in dust continuum modeling. In addition, observations have limitations due to optical depth in molecular lines and the presence of foreground or background structures. Continuum observations with both single dishes and interferometers are insensitive to large-scale structures due to beam switching in the single-dish case and lack of very short spacings in the interferometer data.

More serious difficulties arise, however, because sources are not as simple as the model assumptions. Source geometry is a significant issue. Nearly all young embedded stars have outflows, which create cavities in the envelope and walls at the envelope-outflow boundary; one or more circumstellar disks may be present within the envelope; circumbinary structures may surround systems. These geometrical considerations affect any method for deriving broad envelope structure and require extensive auxiliary information to constrain models. Molecular line tracers are subject to abundance variations driven by outflow shocks, gas heating, grain mantle evaporation, and depletions of gas-phase molecules onto grains. These abundance variations can be factors of 10 or greater, causing selected shocked gas to light up or regions of molecular depletion to disappear completely (van Dishoeck and Blake, 1998). The use of dust emission to probe envelope structure may suffer related difficulties, because grain properties can change as a function of position in the envelope due to grain mantle accumulation and grain-grain coagulation.

All these complications limit the derivation of definitive envelope properties. To first order, $\rho \propto r^{-1.5}$ to r^{-2} often provides a reasonable fit to most data, but it is difficult to distinguish between $r^{-1.5}$ to r^{-2} density profiles or to establish the radius at which $r^{-1.5}$ infall envelopes switch over to r^{-2} as expected in most dynamical models (Foster and Chevalier 1993; Shu et al. 1993). There are indications that some systems may have r^{-1} density gradients in their envelopes (Chandler et al. 1998), but more detailed studies of these systems are needed. Temperature gradients derived from self-consistent radiative transfer models yield reasonable matches to the observed spectral energy distribution. Continued detailed observations and modeling are needed to improve our understanding of envelope structure further.

IV. EARLY DISK AND ENVELOPE EVOLUTION

The evolution of the mass and size of the envelope and disk is broadly understood but only modestly constrained in detail by observations to date. At the simplest level, the envelope starts as the dominant mass component, and its mass must decrease with time in order to produce eventually an optically visible star. Dynamical models of envelope collapse (Larson 1969;

Penston 1969; Shu 1977; Hunter 1977; Foster and Chevalier 1993; Shu et al. 1993) all suggest that the envelope starts with $\rho \propto r^{-2}$ over most (or all) of its extent. As dynamical collapse of the central region progresses, a free-fall density profile, $\rho \propto r^{-1.5}$, develops and moves out into the envelope. For the inside-out model collapse of Shu and collaborators, the density at fixed radius within the infall region evolves as $\rho(\text{fixed } r) \propto (t)^{-1/2}$, where t is time. From an observational viewpoint, this means that the mass within a given beam evolves roughly as $(\text{time})^{-1/2}$, once the free-fall region encompasses the beam. The mass evolution in other models, though not so simple, follows a similar trend. Of course, outflows also clear out envelope material, but their importance to early envelope evolution is dependent on the collimation of the stellar outflow.

The expected evolution of a disk is less well understood than for an envelope. The centrifugal radius (the radius at which centrifugal support from rotation in the parent core becomes important) sets a characteristic disk size. However, the size and mass of a disk should be initially small and increase with time, as progressively higher-angular-momentum material falls into the center of the system and as angular momentum from earlier infall material is redistributed (Terebey et al. 1984; Ruden and Lin 1986; Lin and Pringle 1990). The predicted sizes for disks are in the range of tens to a few hundred AU, but the detailed surface density distribution and size depend on the angular momentum content of the infall material, the viscosity of the material within the disk, and the nature of the processes that control angular momentum redistribution within the disk (Cassen and Moosman 1981; Stahler et al. 1994). None of these are well enough understood to make definitive disk models.

The data to date are sufficient to illustrate broad trends in the evolution. Dividing sources according to the class designation (Adams et al. 1987; André et al. 1993), there is a clear trend of decreasing envelope mass with increasing class numeral (André and Montmerle 1994; Ohashi et al. 1997*a,b*; Hogerheijde et al. 1997; Ladd et al. 1998). This can be roughly represented as

Class 0: $M_{\rm env} \sim 0.2$–$3\ M_\odot$
Class I: $M_{\rm env} \sim 0.02$–$0.3\ M_\odot$
Class II: $M_{\rm env} \leq 0.03\ M_\odot$

Although the class system is a rough evolutionary sequence, it does not provide a pure comparison between envelope mass and age, because the definitions of the classes refer in part to the amount of emission from the envelope. It is, however, the best that can be done until independent age estimates can be made for embedded systems.

Typical disk masses can likewise be estimated for different classes. The masses are best known for Class II sources, where the typical value is $\sim 0.02\ M_\odot$ (Beckwith et al. 1990; André and Montmerle 1994; Osterloh and Beckwith 1995). Less data exist for Class I and Class I/II sources, but

typical disk masses appear to be similar to those of Class II sources (Terebey et al. 1993; Osterloh and Beckwith 1995). Disk masses are poorly determined for Class 0 sources because of the difficulty of separating the disk and envelope components, but it appears that their disks are not significantly more massive than for Class I and II sources (Looney et al. 1998). The disks in Class 0 sources are typically $\leq 10\%$ as massive as their envelopes. Based on the Class II sources, which have the most measurements, there is a large range in disk mass within a class. This range may be associated with age, but it more likely depends on several additional factors, including the angular momentum content of the parent core and multiplicity of the system.

These broad estimates for envelope and disk masses support the expected trend: The circumstellar mass in Class 0 and I systems is dominated by the envelope; Class I to II transition objects have comparably massive envelopes and disks; and the disk dominates the circumstellar mass in Class II systems. This trend is also supported by detailed studies of individual systems (Terebey et al. 1993; Looney et al. 1998). Unfortunately, the time evolution of the disk mass is not well constrained by the observations. There does not appear to be an embedded phase during which low-mass stars have a massive disk (or at least that phase must be very short-lived), but it is not yet clear whether disk mass builds up monotonically throughout the lifetime of the envelope. Scenarios in which the disk mass varies nonmonotonically with time because of accretion events are not ruled out (Bell and Lin 1994; Hartmann and Kenyon 1996).

Measurements of disk and envelope sizes are problematic due to the nature of power law distributions. Observations are now beginning to resolve circumstellar disks in nearby young systems (Lay et al. 1994, 1997; Mundy et al. 1996; Wilner et al. 1996; chapter by Wilner and Lay, this volume); however, the estimated outer radius of the disk depends on the steepness of the power law surface density distribution. Typical values are from 70 to 160 AU radius, with the outer radius poorly constrained for steeper surface density profiles. The definition of the outer radius is further complicated by molecular observations, which typically find disk sizes of 500 to 800 AU (see section V). Envelope outer radii are also poorly defined because of the power law nature of the density profile, but some systems may show discrete outer boundaries (Motte et al. 1998). A systematic approach to quantifying disk and envelope sizes is essential to make progress on understanding the evolution of size.

More high-resolution surveys are needed to establish better the properties of disks and envelopes, and how they evolve. Differences in the properties of single vs. multiple systems are largely unknown for Class 0 and Class I sources because it has been difficult to identify which systems are multiple. Disk properties of Class II sources can be affected by the multiplicity of a system (Beckwith et al. 1990; Jensen et al. 1994, 1996; Osterloh and Beckwith 1995; chapter by Mathieu et al., this volume), but

it is unclear whether disk, and perhaps envelope, properties of multiple systems are different during earlier evolutionary stages.

V. DISK KINEMATICS

Observational studies of disk kinematics have advanced significantly in the past five years, primarily due to increases in the resolution and sensitivity of the millimeter wavelength arrays. The first solid observations of Keplerian rotation in a circumstellar disk were made for the HL Tauri system (Sargent and Beckwith 1987, 1991). This result confirmed the simple theoretical expectation that stable circumstellar disks, unless significant in mass compared to the star, should exhibit nearly Keplerian rotation. Deviations from Keplerian motion are expected because of the transport of material inward onto the star, but within a rotationally supported disk those velocities should be a small fraction of the basic orbital speed unless the disk is dynamically unstable.

There are, however, additional velocity fields present in the inner few hundred AU of a stellar system. The HL Tauri system illustrates these complications. Subsequent observations of the HL Tauri system by Hayashi et al. (1993) found that the velocities were predominantly inflow motions rather than rotation. They fitted a rotation speed of 0.2 km s^{-1} at 700 AU and an infall motion of 1 km s^{-1}, consistent with the outer disk dynamically accreting onto the inner disk and star. The key distinction between the velocity fields arising from rotation and infall is the orientation of the velocity gradient: For rotation the strongest velocity gradient is along the major axis, whereas for infall it is along the minor axis of the projected disk. Clear discussions of the kinematics of rotation and infall are given by Beckwith and Sargent (1993) and Ohashi et al. (1997*b*). The stellar outflow is another source of kinematics that must be considered. Cabrit et al. (1996) argue that the velocity field seen in their images of the HL Tauri system is likely a combination of infall and outflow motion, where the outflow motion arises from material that has been entrained in the stellar jet. Unfortunately, the outflow motions of entrained material are not necessarily as systematic as rotational motions and hence are more difficult to disentangle. Thus, in general, it is necessary to consider rotational, infall, and outflow motions as possibilities. Surveys of the kinematics of T Tauri systems indicate that rotation generally dominates, but a wide variety of velocity fields are seen (Koerner and Sargent 1995; D. W. Koerner and A. I. Sargent, personal communication, 1998).

The best Keplerian velocity curves have been found for optical T Tauri star (Class II) systems, where the lack of a significant envelope minimizes the material involved in infall or outflow activity. Three good examples of Keplerian rotation are provided by the recent observations of the DM Tau, GM Aur, and LkCa 15 systems. The DM Tau system is well fitted by pure Keplerian rotation ($V \propto r^{-0.5\pm0.1}$), with an outer disk radius of 525 AU and a stellar mass of 0.6–0.85 $M_\odot$ (Dutrey et al. 1998). The DM Tau ve-

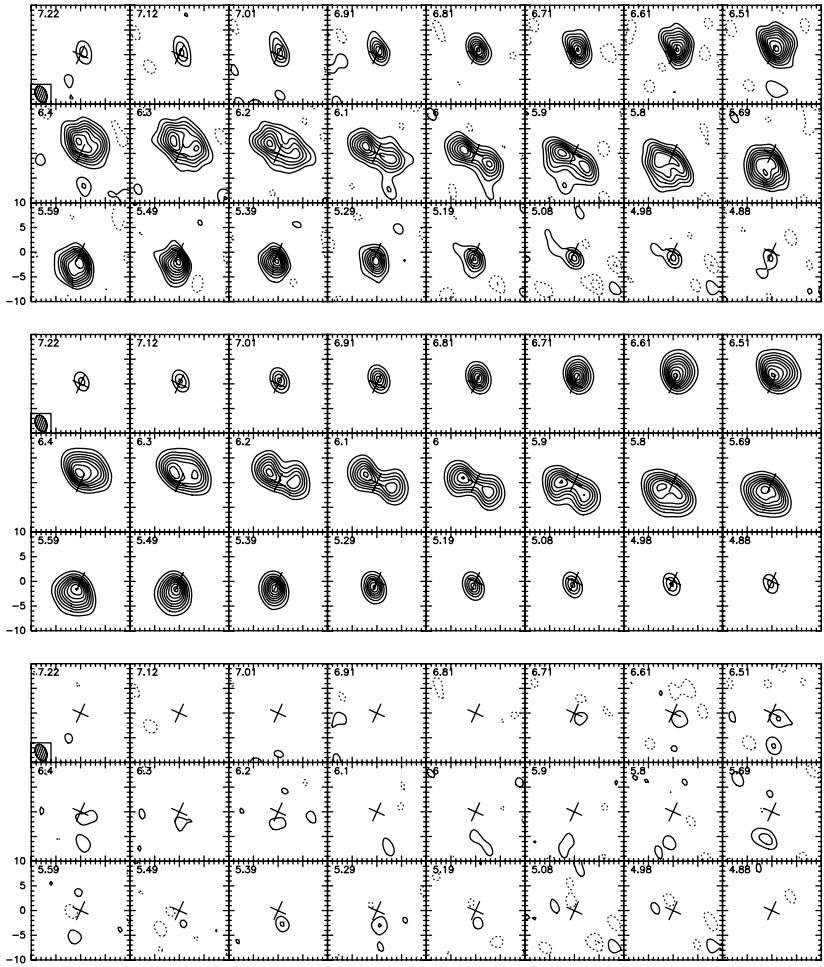

Figure 6. Images of the CO $J = 2$–1 emission, model, and residuals for the DM Tauri system from Guilloteau and Dutrey (1998). The upper set of panels shows the observed emission, with each panel labeled with velocity. The middle panels display the emission from the best-fitted model. The lower panels display the differences between the observations and the model. The angular resolution of the observations is $3.5 \times 2.4''$.

locity field, shown in Fig. 6, is well represented by Keplerian rotation with an outer disk radius of 850 AU and a central stellar mass of 0.4–0.6 $M_\odot$ (Guilloteau and Dutrey 1998). The LkCa 15 velocity field, shown in Fig. 7, is consistent with Keplerian rotation with an outer radius of 220 AU and a central stellar mass of 0.7 $M_\odot$ (A. I. Sargent and D. W. Koerner, personal communication, 1998). As displayed in Figs. 6 and 7, these papers fit velocity channel images, so they are able to set limits on other non-Keplerian motions. For DM Tau, Guilloteau and Dutrey (1998) find that the residual turbulent component of the velocity field is $\sim$0.1 km sec^{-1}, or

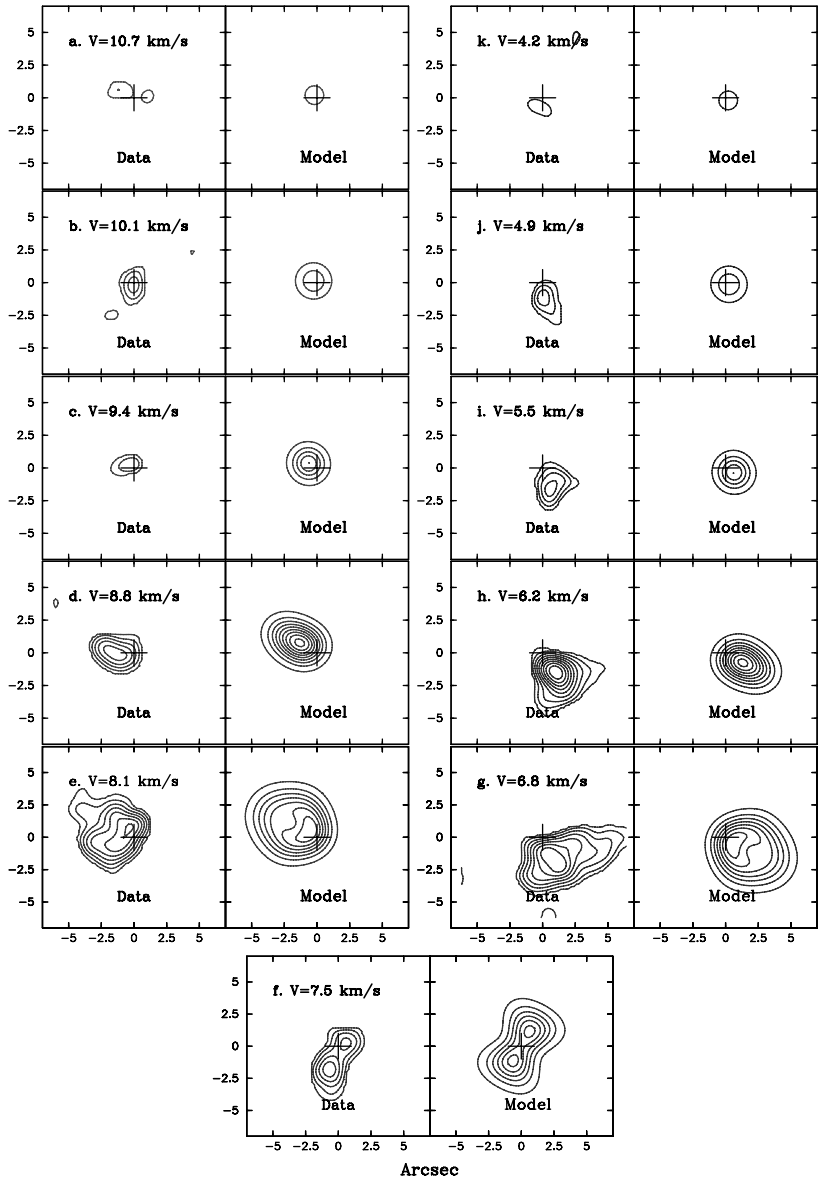

Figure 7. Images of the CO emission and models for the LkCa 15 system from Sargent and Koerner (in preparation). For each pair of panels, the observations are on the left and the model on the right. The panels are labeled with velocity.

0.2–0.3 times the expected thermal width. All these disks are rotationally supported over most, if not all, of their extent.

Systems with even modest envelopes show much more complicated velocity structure and morphology. Observations of three IRAS sources

embedded in the Taurus cloud (Ohashi et al. 1997*a,b*) show thick disk-like structures with sizes (diameters) of 1400 to 2200 AU that are oriented perpendicular to the outflow axes. In two of the sources, the velocity field is argued to be a combination of rotation and infall with infall dominant; in the third case, the motion is consistent with rotation. One of these sources, L1527 (IRAS 04368+2557), shows a central "X" structure, which is likely associated with the cavity walls of the outflow. The L1551 IRS5 system also has a central elongated structure 2400 AU in size that is dominated by infall motions, with lesser rotational motion (Momose et al. 1998); it is argued that the flattened envelope is infalling at a diluted free-fall speed (due to pressure or magnetic support) into a rotationally supported disk inside the centrifugal radius. A more deeply embedded (Class 0) system studied by Gueth et al. (1997), L1157, shows weak evidence of rotation in the inner-500-AU flattened core and evidence of infall and outflow interaction in the surrounding envelope. The coherent progression of structures seen in these systems allows a simple picture of infall and rotation. On the 700- to 1500-AU radial scale, the envelope falls into a flattened, thick disk. Material within this thick disk is primarily infalling but has a modest rotational component. The molecular disk on scales from 200 to 800 AU is composed of infalling material with high specific angular momentum and material that has acquired high angular momentum from transport mechanisms within the disk. Most of the infalling material falls onto the disk at radii less than 150 AU and moves inward within the disk, corresponding to the compact disk observed in the continuum. This picture qualitatively matches the expectations of collapse models with significant rotational or magnetic support (Terebey et al. 1984; Li and Shu 1997; Galli and Shu 1993; Fiedler and Mouschovias 1993). The different scales of structure are linked: the large-scale molecular disk traces the small fraction of material that has high angular momentum; the small-scale continuum disk traces the bulk of the material. These two sizescales are divided observationally, because continuum observations have difficulty imaging the large-scale disk due to the low surface density, whereas the CO and isotopic CO observations have difficulty seeing the inner 80–100 AU of the disk due to the lines becoming optically thick. The quantitative exploration of the connection between the disks traced by CO and continuum emission is a project for the future.

VI. SUMMARY AND CONCLUSIONS

1. Evidence of core fragmentation is seen on a range of scales. The broad morphology of cores fits with current ideas about prompt fragmentation, fragmentation during collapse, and high-angular-momentum scenarios. We suggest that there are natural scales of multiplicity in young embedded systems: separate envelope systems on scales ≥ 6000 AU, common envelope systems on scales from 150 to 3000 AU, and common disk systems on scales ≤ 100 AU.

2. It is difficult to determine the density structure of envelopes with embedded sources accurately. Radial density dependences of $r^{-1.5}$ to r^{-2} are consistent with the data for most young systems, but other power law indexes can also fit. Better observational measurements of the radial density are needed to test current theoretical models, but this will not be easy. The presence of disks, outflows, and multiple structures on different scales, as well as the possibility of multiplicity, complicate the source geometry. The likelihood of strong molecular abundance variations, and the possibility of significant alterations of grain properties within circumstellar material also affect the integrity of the standard molecular and continuum probes.

3. It is clear that envelope mass decreases in going from Class 0 to Class I to Class II sources, but it is unclear how uniquely and precisely that trend is related to age. Current evidence suggests that disk masses in Class I and classical T Tauri systems are not very different. Disk masses in embedded systems are problematic because of the strong envelope emission; the current best estimate is that their disks are not significantly more massive than those in Class I or Class II sources. The time evolution of envelope and disk masses is still an uncertain area that needs more work.

4. Kinematic studies of molecular disks are revealing rotational and infall motions. In some systems, the infall motion is quite significant; in others, pure Keplerian rotation is seen. Pure Keplerian disks with outer radii of 200–800 AU have been measured in several T Tauri systems. The observations support a simple picture in which these large-scale Keplerian disks seen in molecules are high-angular-momentum extensions of the smaller-scale, more massive disks seen in continuum emission. The flattened structures 1000 to 2000 AU in size in embedded systems appear to be partially supported envelopes that are feeding material onto the interior disk structures. More observational studies are needed to solidify these connections and quantify the properties and evolution of the structures.

Acknowledgments We thank A. Sargent, A. Dutrey, D. Koerner, S. Stahler, and C. Chandler for comments and conversations. We give a special thanks to P. André for his critical reading of the text. We thank A. Sargent, D. Koerner, A. Dutrey, and G. Sandell for providing figures from their recent works. We acknowledge support for this work from NSF grant 96-13716 and NASA Origins grant NAG-54429.

REFERENCES

Adams, F. C. 1991. Asymptotic theory for the spatial distribution of protostellar emission. *Astrophys. J.* 382:544–554.

Adams, F. C., Lada, C. J., and Shu, F. C. 1987. Spectral evolution of young stellar objects. *Astrophys. J.* 312:788–806.

André, P., and Montmerle, T. 1994. From T Tauri stars to protostars: Circumstellar material and young stellar objects in the ρ Ophiuchi cloud. *Astrophys. J.* 420:837–862.

André, P., Ward-Thompson, D., and Barsony, M. 1993. Submillimeter continuum observations of ρ Ophiuchi A: The candidate protostar VLA 1623 and prestellar clumps. *Astrophys. J.* 406:122–141.

Artymowicz, P., and Lubow, S. H. 1994. Dynamics of binary-disk interaction. I: Resonances and disk gap sizes. *Astrophys. J.* 421:651–667.

Bachiller, R., Guilloteau, S., Gueth, F., Tafalla, M., Dutrey, A., Codella, C., and Castets, A. 1998. A molecular jet from SVS 13B near HH 7–11. *Astron. Astrophys.* 339:L49–L52.

Bate, M. R., and Bonnell, I. A. 1997. Accretion during binary star formation. II: Gaseous accretion and disc formation. *Mon. Not. Roy. Astron. Soc.* 285:33–48.

Beckwith, S. V. W., and Sargent, A. I. 1993. Molecular line emission from circumstellar disks. *Astrophys. J.* 402:280–291.

Beckwith, S. V. W., Sargent, A. I., Chini, R. S., and Guesten, R. 1990. A survey of circumstellar disks around young stellar objects. *Astron. J.* 99:924–945.

Bell, K. R., and Lin, D. N. C. 1994. Using FU Orionis outbursts to constrain self-regulated protostellar disk models. *Astrophys. J.* 427:987–1004.

Bertoldi, F., and McKee, C. F. 1992. Pressure-confined clumps in magnetized molecular clouds. *Astrophys. J.* 395:140–157.

Bonnell, I., Martel, H., Bastien, P., Arcoragi, J-P., and Benz, W. 1991. Fragmentation of elongated cylindrical clouds. III: Formation of binary and multiple systems. *Astrophys. J.* 377:553–558.

Bonnell, I. A., Bate, M. R., Clarke, C. J., and Pringle, J. E. 1997. Accretion and the stellar mass spectrum in small clusters. *Mon. Not. Roy. Astron. Soc.* 285:201–208.

Boss, A. 1995. Gravitational collapse and binary protostars. *Rev. Mex. Astron. Astrofis.* 1:165–177.

Boss, A. P. 1997. Collapse and fragmentation of molecular cloud cores. V: Loss of magnetic field support. *Astrophys. J.* 483:309–319.

Burkert, A., and Bodenheimer, P. 1993. Multiple fragmentation in collapsing protostars. *Mon. Not. Roy. Astron. Soc.* 264:798–806.

Butner, H. M., Natta, A., and Evans II, N. J. 1994. Spherical disks: Moving toward a unified source model for L1551. *Astrophys. J.* 420:326–335.

Cabrit, S., Guilloteau, S., André, P., Bertout, C., Montmerle, T., and Schuster, K. 1996. Plateau de Bure observations of HL Tauri: Outflow motions in a remnant circumstellar envelope. *Astron. Astrophys.* 305:527–540.

Cassen, P., and Moosman, A. 1981. On the formation of protostellar disks. *Icarus* 48:353–376.

Chandler, C. J., Barsony, M., and Moore, T. J. T. 1998. The circumstellar envelopes around three protostars in Taurus. *Mon. Not. Roy. Astron. Soc.* 299:789–798.

Chini, R., Reipurth, B., Sievers, A., Ward-Thompson, D., Haslam, C. G. T., Kreysa, E., and Lemke, R. 1997. Cold dust around Herbig-Haro energy sources: Morphology and new protostellar candidates. *Astron. Astrophys.* 325:542–550.

Choi, M., Evans II, N. J., Gregersen, E. M., and Wang, Y. 1995. Modeling line profiles of protostellar collapse in B335 with the Monte Carlo method. *Astrophys. J.* 448:742–747.

Duquennoy, A., and Mayor, M. 1991. Multiplicity among solar type stars in the solar neighborhood. II: Distribution of the orbital elements in an unbiased sample. *Astron. Astrophys.* 248:485–524.

Dutrey, A., Guilloteau, S., Prato, L., Simon, M., Duvert, G., Schuster, K., and Menard, F. 1998. CO study of the GM Aurigae Keplerian disk. *Astron. Astrophys.* 338:L63–L66.

Fiedler, R. A., and Mouschovias, T. C. 1993. Ambipolar diffusion and star formation: Formation and contraction of axisymmetric cloud cores. II: Results. *Astrophys. J.* 415:680–700.

Foster, P. N., and Chevalier, R. A. 1993. Gravitational collapse of an isothermal sphere. *Astrophys. J.* 416:303–311.

Fuller, G. A., Ladd, E. F., Padman, R., Myers, P. C., and Adams, F. C. 1995. The circumstellar molecular core around L1551 IRS 5. *Astrophys. J.* 454:862–871.

Galli, D., and Shu, F. H. 1993. Collapse of magnetized molecular cloud cores. II: Numerical results. *Astrophys. J.* 417:243–258.

Ghez, A., McCarthy, D. W., Patience, J. L., and Beck, T. L. 1997. The multiplicity of pre-main-sequence stars in southern star-forming regions. *Astrophys. J.* 481:378–385.

Gomez, M., Hartmann, L., Kenyon, S. J., and Hewett, R. 1993. On the spatial distribution of pre-main-sequence stars in Taurus. *Astron. J.* 105:1927–1937.

Gueth, F., Guilloteau, S., Dutrey, A., and Bachiller, R. 1997. Structure and kinematics of a protostar: mm-interferometry of L1157. *Astron. Astrophys.* 323:943–952.

Guilloteau, S., and Dutrey, A. 1998. Physical parameters of the Keplerian protoplanetary disk of DM Tauri. *Astron. Astrophys.* 339:467–476.

Hartmann, L., and Kenyon, S. J. 1996. The FU Orionis phenomenon. *Ann. Rev. Astron. Astrophys.* 34:207–240.

Hayashi, M., Ohashi, N., and Miyama, S. M. 1993. A dynamically accreting gas disk around HL Tau. *Astrophys. J. Lett.* 418:L71–L74.

Hogerheijde, M. R., van Dishoeck, E. F., Blake, G. A., and van Langevelde, H. J. 1997. Tracing the envelope around embedded low-mass young stellar objects with HCO^+ and millimeter continuum observations. *Astrophys. J.* 489:293–313.

Hunter, C. 1977. The collapse of unstable isothermal spheres. *Astrophys. J.* 218:834–845.

Jensen, E. L. N., Mathieu, R. D., and Fuller, G. A. 1994. A connection between submillimeter continuum flux and separation in young binaries. *Astrophys. J. Lett.* 429:L29–L32.

Jensen, E. L. N., Mathieu, R. D., and Fuller, G. A. 1996. The connection between submillimeter continuum flux and binary separation in young binaries: Evidence for interaction between stars and disks. *Astrophys. J.* 458:312–326.

Keene, J., and Masson, C. R. 1990. Detection of a 45 AU radius source around L1551-IRS5: A possible accretion disk. *Astrophys. J.* 355:635–644.

Koerner, D. W., and Sargent, A. I. 1995. Imaging the small-scale circumstellar gas around T Tauri stars. *Astron. J.* 109:2138–2145.

Ladd, E. F., Fuller, G. A., and Deane, J. R. 1998. $C^{18}O$ and $C^{17}O$ observations of embedded young stars in the Taurus molecular cloud. I: Integrated intensities and column densities. *Astrophys. J.* 495:871–890.

Larson, R. B. 1969. Numerical calculations of the dynamics of a collapsing protostar. *Mon. Not. Roy. Astron. Soc.* 145:271–295.

Larson, R. B. 1978. Calculations of three-dimensional collapse and fragmentation. *Mon. Not. Roy. Astron. Soc.* 184:69–85.

Larson, R. B. 1995. Star formation in groups. *Mon. Not. Roy. Astron. Soc.* 272:213–220.

Lay, O. P., Carlstrom, J. E., Hills, R. E., and Phillips, T. G. 1994. Protostellar accretion disks resolved with the CSO-JCMT interferometer. *Astrophys. J. Lett.* 434:L75–L78.

Lay, O. P., Carlstrom, J. E., and Hills, R. E. 1995. NGC1333 IRAS 4: Further multiplicity revealed with the CSO-JCMT interferometer. *Astrophys. J. Lett.* 452:L73–L76.

Lay, O. P., Carlstrom, J. E., and Hills, R. E. 1997. Constraints on the HL Tauri protostellar disk from millimeter and submillimeter wave interferometry. *Astrophys. J.* 489:917–927.

Lefloch, B., Castets, A., Cernicharo, J., Langer, W. D., and Zylka, R. 1998. Cores and cavities in NGC 1333. *Astron. Astrophys.* 334:269–279.

Li, Z. Y., and Shu, F. H. 1997. Self-similar collapse of an isopedic isothermal disk. *Astrophys. J.* 475:237–250.

Lin, D. N. C., and Pringle, J. E. 1990. The formation and initial evolution of protostellar disks. *Astrophys. J.* 358:515–524.

Looney, L. W., Mundy, L. G., and Welch, W. J. 1997. High-resolution $\lambda = 2.7$ millimeter observations of L1551 IRS 5. *Astrophys. J. Lett.* 484:L157–L160.

Looney, L. W., Mundy, L. G., and Welch, W. J. 1998. Unveiling the envelope and disk: A sub-arcsecond survey. *Astrophys. J.,* submitted.

Men'shchikov, A. B., and Henning, T. 1997. Radiative transfer in circumstellar disks. *Astron. Astrophys.* 318:879–907.

Momose, M., Ohashi, N., Kawabe, R., Nakano, T., and Hayashi, M. 1998. Aperture synthesis $C^{18}O$ $J = 1$–0 observations of L1551 IRS5: Detailed structure of the infalling envelope. *Astrophys. J.* 504:314–333.

Motte, F. 1998. Structure des coeurs denses proto-stellaires: Etude en continuum millimetrique. Ph.D. thesis. *J. Astron. Francais* 57:82.

Motte, F., André, P., and Neri, R. 1998. The initial conditions of star formation in the ρ Ophiuchi main cloud: Wide-field millimeter continuum mapping. *Astron. Astrophys.* 336:150–172.

Mundy, L. G., Looney, L. W., Erickson, W., Grossman, A., Welch, W. J., Forster, J. R., Wright, M. C. H., Plambeck, R. L., Lugten, J., and Thornton, D. D. 1996. Imaging the HL Tauri disk at $\lambda = 2.7$ millimeters with the BIMA array. *Astrophys. J. Lett.* 464:L169–L172.

Nakajima, Y., Tachihara, K., Hanawa, T., and Nakano, M. 1998. Clustering of pre-main-sequence stars in the Orion, Ophiuchus, Chamaeleon, Vela, and Lupus star-forming regions. *Astrophys. J.* 497:721–735.

Narayanan, G., Walker, C. K., and Buckley, H. D. 1998. *Astrophys. J.* 496:292–310.

Ohashi, N., Masahiko, H., Ho, P. T. P., Momose, M., Tamura, M., Hirano, N., and Sargent, A. I. 1997*a*. Rotation in the protostellar envelopes around IRAS 04169+2702 and IRAS 04365+2535: The size scale for dynamical collapse. *Astrophys. J.* 488:317–329.

Ohashi, N., Hayashi, M., Ho, P. T. P., and Momose, M. 1997*b*. Interferometric imaging of IRAS 04368+2557 in the L1527 molecular cloud core: A dynamically infalling envelope with rotation. *Astrophys. J.* 475:211–223.

Osterloh, M., and Beckwith, S. V. W. 1995. Millimeter-wave continuum measurements of young stars. *Astrophys. J.* 439:288–302.

Patience, J., Ghez, A. M., Reid, I. N., Weinberger, A. J., and Matthews, K. 1998. The multiplicity of the Hyades and its implications for binary star formation and evolution. *Astron. J.* 115:1972–1988.

Penston, M. V. 1969. Dynamics of self-gravitating gaseous spheres. III. *Mon. Not. Roy. Astron. Soc.* 144:425–448.

Pringle, J. E. 1989. On the formation of binary stars. *Mon. Not. Roy. Astron. Soc.* 239:361–370.

Rodriguez, L. F., D'Alessio, P., Wilner, D. J., Ho, P. T. P., Torrelles, J. M., Curiel, S., Gomez, Y., Lizano, S., Pedlar, A., Canto, J., and Raga, A. C. 1998. Compact protoplanetary disks in a binary system in L1551. *Nature* 395:355–357.

Rowan-Robinson, M. 1980. Radiative transfer in dust clouds. I: Hot-centered clouds associated with regions of massive star formation. *Astrophys. J. Suppl.* 44:403–426.

Ruden, S. P., and Lin, D. N. C. 1996. The global evolution of the primordial solar nebula. *Astrophys. J.* 308:883–901.

Sandell, G., Aspin, C., Duncan, W. D., Russell, A. P. G., and Robson, E. I. 1991. NGC1333 IRAS4: A very young, low-luminosity binary system. *Astrophys. J. Lett.* 376:L17–L20.

Sargent, A. I., and Beckwith, S. V. W. 1987. Kinematics of the circumstellar gas of HL Tauri and R Monocerotis. *Astrophys. J.* 323:294–305.

Sargent, A. I., and Beckwith, S. V. W. 1991. The molecular structure around HL Tauri. *Astrophys. J. Lett.* 382:L31–L35.

Shu, F. H. 1977. Self-similar collapse of isothermal spheres and star formation. *Astrophys. J.* 214:488–497.

Shu, F.H., Najita, J., Galli, D., Ostriker, E., and Lizano, S. 1993. The collapse of clouds and the formation and evolution of stars and disks. In *Protostars and Planets III,* ed. E. H. Levy and J. I. Lunine (Tucson: University of Arizona Press), pp. 3–45.

Simon, M. 1997. Clustering of young stars in Taurus, Ophiuchus, and the Orion Trapezium. *Astrophys. J. Lett.* 482:L81–L84.

Simon, M., Chen, W. P., Howell, R. R., Denson, J. A., and Slowik, D. 1992. Multiplicity among the young stars in Taurus. *Astrophys. J.* 384:212–219.

Stahler, S. W., Korycansky, D. G., Brothers, M. J., and Touma, J. 1994. The early evolution of protostellar disks. *Astrophys. J.* 431:341–358.

Terebey, S., Shu, F. H., and Cassen, P. 1984. The collapse of slowly rotating isothermal clouds. *Astrophys. J.* 286:529–551.

Terebey, S., Chandler, C. J., and André, P. 1993. The contribution of disks and envelopes to the millimeter continuum emission from very young low-mass stars. *Astrophys. J.* 414:759–772.

Testi, L., and Sargent, A. I. 1998. Star formation in clusters: A survey of compact millimeter-wave sources in the Serpens core. *Astrophys. J. Lett.* 508:L91–L94.

van Dishoeck, E. F., and Blake, G. A. 1998. Chemical evolution of star-forming regions. *Ann. Rev. Astron. Astrophys.* 36:317–368.

Walker, C. K., Adams, F. C., and Lada, C. J. 1990. 1.3-millimeter continuum observations of cold molecular cloud cores. *Astrophys. J.* 349:515–528.

Welch, W. J., Mundy, L. G., and Looney, L. W. 1999. *Astrophys. J.,* in preparation.

Williams, J. P., and Blitz, L. 1998. A multitransition CO and CS (2–1) comparison of a star-forming and a non-star-forming giant molecular cloud. *Astrophys. J.* 491:657–673.

Wilner, D. J., Welch, W. J., and Forster, J. R. 1995. Sub-arcsecond imaging of W3(OH) at 87.7 GHz. *Astrophys. J. Lett.* 449:L73–L76.

Wilner, D. J., Ho, P. T. P., and Rodriguez, L. F. 1996. Subarcsecond VLA observations of HL Tauri: Imaging the circumstellar disk. *Astrophys. J. Lett.* 470:L117–L121.

Wolfire, M. G., and Cassinelli, J. P. 1986. The temperature structure in accretion flows into massive protostars. *Astrophys. J.* 310:207–221.

Yun, J. L., and Clemens, D. P. 1991. Radial dust density profiles in small molecular clouds. *Astrophys. J.* 381:474–483.

Zhou, S., Evans, N. J., II, Kompe, C., and Walmsley, C. M. 1993. Evidence for protostellar collapse in B335. *Astrophys. J.* 404:232–246.

Zhou, S. 1995. Line formation in collapsing cloud cores with rotation and applications to B335 and IRAS 16293−2422. *Astrophys. J.* 442:685–693.